Group-theory analysis of electrons and phonons in *N*-layer graphene systems

L. M. Malard, M. H. D. Guimarães, D. L. Mafra, M. S. C. Mazzoni, and A. Jorio
Departamento de Física, Universidade Federal de Minas Gerais, 31270-901, Belo Horizonte, Brazil
(Received 5 December 2008; revised manuscript received 20 January 2009; published 23 March 2009)

In this work we study the symmetry properties of electrons and phonons in graphene systems as a function of the number of layers. We derive the selection rules for the electron-radiation interactions and for the electron-phonon interactions at all points in the Brillouin zone. By considering these selection rules, we address the double-resonance Raman-scattering process. The monolayer and bilayer graphenes in the presence of an applied electric field are also discussed.

DOI: 10.1103/PhysRevB.79.125426 PACS number(s): 02.20.−a, 78.30.−j, 78.67.−n

I. INTRODUCTION

The current interest on graphene and its multilayered materials has been stimulated by various experimental and theoretical works addressing the physics of Dirac fermions and the potential for device applications (Refs. 1 and 2, and references therein). Group theory is a powerful theoretical tool to determine eigenvectors, the number and the degeneracies of eigenvalues, and to obtain and understand the selection rules governing, for example, electron-radiation and electron-phonon interactions. Although the symmetry aspects of monolayer graphene and graphite have been largely discussed in the literature,[3] recent findings generate interest in a group theory analysis depending on the number of graphene layers.

This work presents a group theory analysis for electrons and phonons in monolayer, bilayer, and trilayer graphenes, extending for *N* layers depending if *N* is even or odd, all with Bernal (AB) stacking. The selection rules for electron-radiation interaction within the dipole approximation and for electron scattering by phonons are derived. With these selection rules, we discuss the double-resonance Raman (DRR) scattering process, which has been widely used to characterize the number of layers,[4–6] and to probe their electronic and vibrational properties.[7–9] Finally, we also discuss the differences when monolayer and bilayer graphenes are exposed to external electrical fields, giving insight on the gap opening in the biased bilayer graphene[10–14] and different selection rules for the electron-phonon scattering (EPS) process.

Section II gives the symmetry properties for monolayer and *N*-layer graphenes depending if *N* is even or odd. The monolayer and bilayer graphenes are also considered in the presence of an electric field perpendicular to the graphene plane. The notation adopted is related to the space-group (SG) symmetry, and conversion to the point-group (PG) notation can be found in the Appendix. Section III presents the selection rules for the electron-radiation interaction. Section IV shows the Γ point Raman and infrared (IR)-active modes. We extend the electron-phonon selection rules to points in the interior of the Brillouin zone, and address the DRR process for monolayer, bilayer, and trilayer graphenes in Sec. V. The main findings are summarized in Sec. VI.

II. SYMMETRY PROPERTIES

A. Group of wave vector

Figures 1(a) and 1(d) show the hexagonal real space for the monolayer graphene with two inequivalent atoms in the unit cell. The origin is set at the highest symmetry point, i.e., at the center of a hexagon. The reciprocal space is shown in Fig. 1(g) highlighting the high-symmetry points Γ, *K*, *K′*, and *M*, and lines *T*, *T′*, and Σ. Any other generic point outside the high-symmetry lines and points is named here as *u*. The monolayer graphene on an isotropic medium has the space-group $P6/mmm$ (D_{6h}^1) in the Hermann-Mauguin (Schoenflies) notation. At the Γ point, the group of wave vector (GWV) is isomorphic to the point group D_{6h} (the Schoenflies character tables for the point groups can be found in Ref. 3).

The real space for bilayer and trilayer graphenes with AB Bernal stacking is show in Figs. 1(b) and 1(e), and 1(c) and 1(f), respectively. The symmetries for *N*-layer graphene, with *N* even or odd (from now on, $N \neq 1$), are the same as for bilayer and trilayer graphenes, respectively. The main symmetry operation distinguishing the point groups between even and odd layers are the horizontal mirror plane, which is absent for *N* even, and the inversion, which is absent for *N* odd. The point groups isomorphic to the GWV for monolayer, *N*-layer graphene (*N* even and odd), and for *N* infinite (graphite) are listed in Table I for all points and lines in the first Brillouin zone (BZ). The GWV for *N*-layer graphene are subgroups of the GWV for single layer graphene. The direct product between the group from *N* even and *N* odd gives the graphene GWV, i.e.,

TABLE I. The space groups and wave-vector point groups for monolayer, *N*-layer graphene, and graphite (*N* infinite) at all points in the BZ.

	Space group	Γ	K (K')	M	T (T')	Σ	u
Monolayer	$P6/mmm$	D_{6h}	D_{3h}	D_{2h}	C_{2v}	C_{2v}	C_{1h}
N even	$P\bar{3}m1$	D_{3d}	D_3	C_{2h}	C_2	C_{1v}	C_1
N odd	$P\bar{6}m2$	D_{3h}	C_{3h}	C_{2v}	C_{1h}	C_{2v}	C_{1h}
N infinite	$P6_3/mmc$	D_{6h}	D_{3h}	D_{2h}	C_{2v}	C_{2v}	C_{1h}

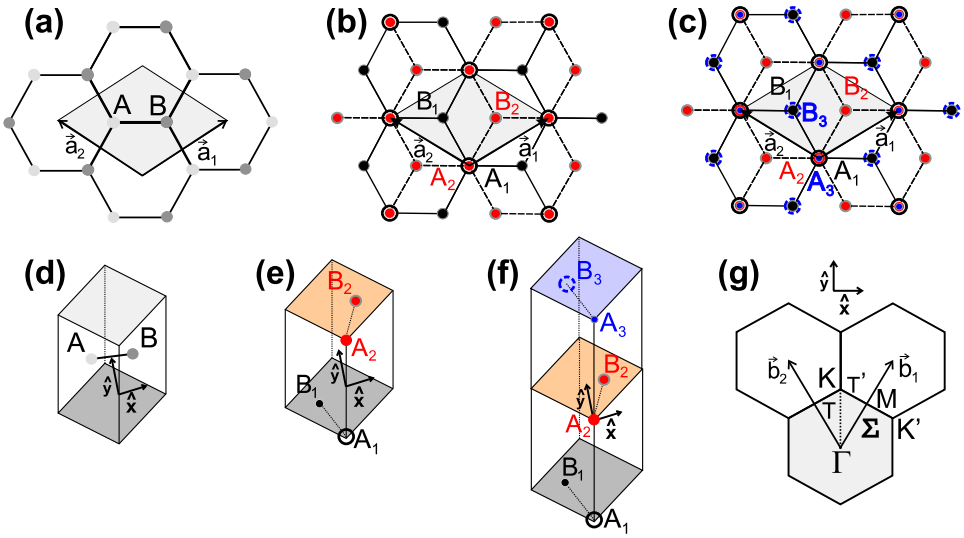

FIG. 1. (Color online) (a) The real-space topview of a monolayer graphene showing the nonequivalent *A* and *B* atoms. (b) The real-space topview of bilayer graphene. Black dots plus black open circles, and light gray (red) dots represent the atoms in the lower and upper layers, respectively. (c) The real topview trilayer graphene. Black dots plus black open circles, light gray (red) dots, and dark gray (blue) dots plus traced dark gray (blue) circles represent the atoms in the lower, middle, and upper layers, respectively. The three dimensional unit cells of (d) monolayer, (e) bilayer, and (f) trilayer graphenes. (g) The reciprocal space showing the first Brillouin zone in light gray, the high-symmetry points and lines, and the two primitive vectors.

$$\{G_{\text{even}}|0\} \otimes \{G_{\text{odd}}|0\} = \{G_{\text{monolayer}}|0\}.$$

On graphite, the wave-vector point groups are isomorphic to the wave-vector point groups of monolayer graphene but differ fundamentally for some classes where a translation of $c/2$ is present, with graphite belonging to the $P6_3/mmc$ (D_{6h}^4) nonsymorphic space group.

B. Lattice vibrations and π electrons

The representations for the lattice vibration ($\Gamma_{\text{lat vib}}$) and for the π electrons (Γ_π) are given by $\Gamma_{\text{lat vib}}=\Gamma^{\text{eq}}\otimes\Gamma^{\text{vector}}$ and $\Gamma_\pi=\Gamma^{\text{eq}}\otimes\Gamma^z$, respectively, where Γ^{eq} is the atom equivalence representation, and Γ^{vector} is the representation for the vectors x, y, and z. For Γ_π we used only Γ^z, which is the irreducible representation for the vector z since π electrons in graphene are formed by p_z electronic orbitals. The results for all points and lines in the first BZ for the $\Gamma_{\text{lat vib}}$ are found in Table II and for the Γ_π in Table III.

Table III shows that the π electrons in monolayer graphene are degenerated at the *K* (Dirac) point, as obtained by theory.[15,16] Figures 2(a)–2(c) show the electronic structure of monolayer, bilayer, and trilayer graphenes, respectively, calculated via density-functional theory (DFT).[17–19] The symmetry assignments of the different electronic branches shown in Fig. 2 were made according to the DFT projected density of states.

The bilayer graphene with AB Bernal stacking [see Figs. 1(b) and 1(e)] is also a zero gap semiconductor composed by two conduction and two valence π bands, and the electrons exhibit a parabolic dispersion near the *K* point. Two bands are degenerated at the *K* point [see Table III and Fig. 2(b)] and the other two have a gap of $2\gamma_1$, where γ_1 is the Slonczewski-Weiss-McClure parameter[20,21] that have an experimental value of ~0.3–0.4 eV.[7,11,22]

Trilayer graphene in the ABA Bernal stacking [see Figs. 1(c) and 1(f)], belongs to the D_{3h} point group and Fig. 2(c)

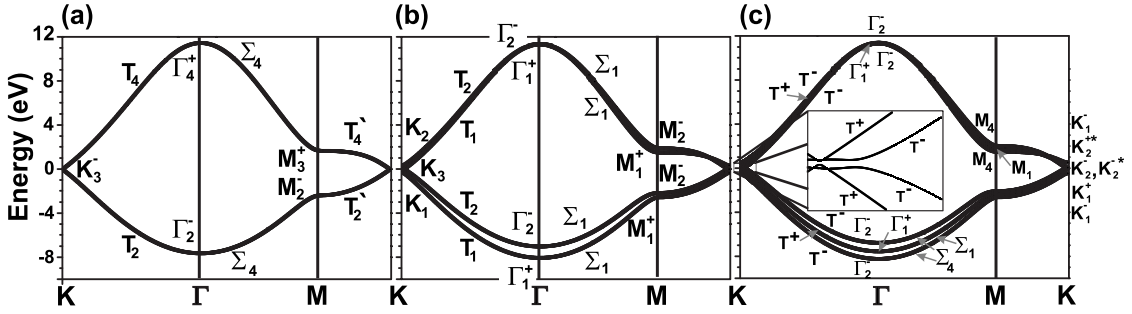

FIG. 2. The electronic dispersion for the π electrons and the irreducible representations (Γ_π) for (a) monolayer, (b) bilayer, and (c) trilayer graphenes along the $K\Gamma MK$ directions. The calculation was done via pseudopotential DFT (Ref. 17) as implemented in the SIESTA program (Refs. 18 and 19). We used a basis set composed of pseudo atomic orbitals of finite range and the local-density approximation (LDA) with the Ceperley-Alder parametrization for the exchange-correlation functional.

TABLE II. The $\Gamma_{\text{lat vib}}$ wave-vector point-group representations for monolayer and N-layer graphenes at all points in the BZ.

	Monolayer	N even	N odd
Γ	$\Gamma_2^-+\Gamma_5^-+\Gamma_4^++\Gamma_6^+$	$N(\Gamma_1^++\Gamma_3^++\Gamma_2^-+\Gamma_3^-)$	$(N-1)\Gamma_1^++(N+1)\Gamma_2^-+(N+1)\Gamma_3^++(N-1)\Gamma_3^-$
K [a]	$K_1^++K_2^++K_3^++K_3^-$	$N(K_1+K_2+2K_3)$	$NK_1^++NK_1^-+[f(N)+2]K_2^++[f(N-2)]K_2^{+*}+NK_2^-+(N-1)K_2^{-*}$ [b]
M	$M_1^++M_2^++M_3^++M_2^-+M_3^-+M_4^-$	$N(2M_1^++M_2^++M_1^-+2M_2^-)$	$2NM_1+(N-1)M_2+(N+1)M_3+2NM_4$
$T(T')$	$2T_1+T_2+2T_3+T_4$	$3N(T_1+T_2)$	$(3N+1)10T^++(3N-1)T^-$
Σ	$2\Sigma_1+2\Sigma_3+2\Sigma_4$	$N(4\Sigma_1+2\Sigma_2)$	$2N\Sigma_1+(N-1)\Sigma_2+(N+1)\Sigma_3+2N\Sigma_4$
u	$4u^++2u^-$	$6Nu$	$(3N+1)u^++(3N-1)u^-$

[a]The K' point irreducible representations are given by the complex conjugate of the K point.
[b]$f(N)=\Sigma_{m=0}^{\infty}[\Theta(N-4m-2)+3\Theta(N-4m-4)]$, where $\Theta(x)$ is equal to 0 if $x<0$ and equal to 1 otherwise.

shows its electronic dispersion. The K point of trilayer is isomorphic to C_{3h}. In Tables II and III, K_2^+ and K_2^{+*} are the two one-dimensional representations of the K_2^+ representation, where $*$ means the complex conjugate. The same happens for the K_2^- representation. The electron representations will be given by $\Gamma_\pi^K=K_1^++2K_1^-+K_2^{+*}+K_2^-+K_2^{-*}$ for the K point and $\Gamma_\pi^{K'}=K_1^++2K_1^-+K_2^++K_2^{-*}+K_2^-$ for K' point. Although time reversion symmetry can imply degeneracies between complex-conjugate representations in cyclic groups, in graphene the complex conjugation also takes K into K' point and, consequently, there are no degenerated bands at the $K(K')$ point, in agreement with *tight-binding* calculations when including the γ_2 and γ_5 next-nearest-layer coupling parameters.[23,24] This energy gap is also obtained from *ab initio* calculations [see the inset of Fig. 2(c) and Ref. 25].

It is worth noting that our work only addresses the AB stacking. Some theoretical works have shown interesting behavior of the Dirac points for the case of ABC stacking,[25,26] where the inversion symmetry is present,[26] and the valence and conduction bands can be degenerated near the K point.[25,26]

C. Gated monolayer and bilayer graphenes

If the monolayer graphene is in the presence of a perpendicular electric field (gated graphene), the Fermi level changes. The presence of charge inhomogeneity caused by substrate and/or absorbed water can generate the same effect as verified in transport[27,28] and Raman measurements,[29] where the Dirac point is shifted from the neutrality point. In these cases, the π electrons lose the horizontal mirror plane and the inversion symmetry, and the system is isomorphic to the point group C_{6v}. The irreducible representations for the Γ_π for the gated graphene can be found in Table IV. The K point electrons still belong to the double-degenerated K_3 irreducible representation, and there is no gap opening at K point for a perfect perpendicular electric-field effect.

The biased bilayer graphene has attracted a lot of attention recently because it is the only material known to have a tunable energy gap,[10–14] promising for applications on devices and lasers with tunable energy. The mechanism behind this feature is based on applying an electric field perpendicular to the graphene layers so that the two layers will be under inequivalent potentials. Then it is possible to open a gap at the K point, breaking the double-degenerated K_3 irreducible representation into two one-dimensional irreducible representations. Since the biased bilayer graphene breaks the inversion center symmetry, the group of the wave vector at Γ for perfect perpendicular electric field is isomorphic to C_{3v}. Table IV shows that the biased bilayer contains the two one-dimensional representations K_2 and K_2^* at the K point, and a gap opening is expected on the basis of symmetry arguments considering inequivalent layers.

The electric field does not affect the symmetries of the phonons. The representations for the $\Gamma_{\text{lat vib}}$ of the gated monolayer (or biased bilayer) are the same as the monolayer (or bilayer) in an isotropic medium, given in Table II.

TABLE III. The Γ_π wave-vector point-group representations for monolayer and N-layer graphenes at all points in the BZ.

	Monolayer	N even	N odd
Γ	$\Gamma_2^-+\Gamma_4^+$	$N(\Gamma_1^++\Gamma_2^-)$	$(N-1)\Gamma_1^++(N+1)\Gamma_2^-$
K [a]	K_3^-	$\frac{N}{2}(K_1+K_2+K_3)$	$(\frac{N-1}{2})K_1^++(\frac{N+1}{2})K_1^-+g(N)K_2^{+*}+g(N-2)K_2^++g(N)K_2^-+g(N+2)K_2^{-*}$ [b]
M	$M_3^++M_2^-$	$N(M_1^++M_2^-)$	$(N-1)M_1+(N+1)M_4$
$T(T')$	T_2+T_4	$N(T_1+T_2)$	$(N-1)T^++(N+1)T^-$
Σ	$2\Sigma_4$	$2N\Sigma_1$	$(N-1)\Sigma_1+(N+1)\Sigma_4$
u	$2u^-$	$2Nu$	$(N-1)u^++(N+1)u^-$

[a]The K' point irreducible representations are given by the complex conjugate of the K point.
[b]$g(N)=\Sigma_{m=0}^{\infty}\Theta(N-4m-2)$, where $\Theta(x)$ is equal to 0 if $x<0$ and equal to 1 otherwise.

III. SELECTION RULES FOR ELECTRON-RADIATION INTERACTION

The symmetry properties described in the previous section will now be applied to physical processes. In this section we discuss the selection rules for electron-radiation interaction in the dipole approximation, with emphasis on the high-symmetry lines T and T' in the electronic dispersion, where interesting phenomena occur.

In the dipole approximation, the absorption of light in a material is related to the wave functions of the electron states in the valence $[\psi^v(\mathbf{k})]$ and conduction $[\psi^c(\mathbf{k})]$ bands, and the polarization of the incoming light $(\mathbf{P})$ by $W(\mathbf{k}) \propto |\mathbf{P}\cdot\langle\psi^c(\mathbf{k})|\nabla|\psi^v(\mathbf{k})\rangle|^2$.[30,31] Knowing the symmetry of the initial and final states, and the representation that generates the basis function of the light polarization vector (x, y, or z), group theory can be used to compute when $W(\mathbf{k})$ is null or not. The results are summarized in Table V considering graphene layers lying in the (x,y) plane and light propagating along z. We will discuss in more details the results of Table V for bilayer and trilayer graphenes since these systems will be used in Sec. V to address the DRR scattering. In the case of graphene, the light absorption up to 3 eV occurs only at T, T', and u points.

It is important to highlight some results given in Table V. In the case of monolayer graphene on an isotropic medium, numerical calculations show an anisotropy in the optical absorption.[31–33] This anisotropy has indeed a symmetry basis, as clearly seen when analyzing the selection rules at the T line. Absorption by visible light has to couple T_2 and T_4 π electron symmetries [see Fig. 2(a)]. For the T line direction along $\hat{y}$, the only allowed absorption is for light polarized along the $\hat{x}$ direction. For incident light polarization along the $\hat{y}$ direction, no absorption will occur along $K\Gamma$ direction, giving rise to the optical-absorption anisotropy on graphene.[31–33] Outside the high-symmetry T line there is a nonzero probability of absorption and the anisotropy is obtained by defining orthogonal basis, as shown in Ref. 31.

When the monolayer graphene is on top of a substrate, with the influence of the environment changing the Fermi level, there will be no change in the selection rules for electron-radiation interaction. Along the T line, the π electrons are described by T_1 and T_2 representations, where T_2 and T_1 contain x and y basis functions, respectively. Again there will be no absorption for y polarization along $K\Gamma$ direction.

TABLE IV. The group of wave vector and its Γ_π representations for gated monolayer and biased bilayer graphenes.

	Gated monolayer		Biased bilayer	
	GWV	Γ_π	GWV	Γ_π
Γ	C_{6v}	$\Gamma_1+\Gamma_4$	C_{3v}	$4\Gamma_1$
$K(K')$	C_{3v}	K_3	C_3	$2K_1+K_2+K_2^*$
M	C_{2v}	M_1+M_3	C_{1v}	$4M_1$
$T(T')$	C_{1v}	T_1+T_2	C_1	$4T$
Σ	C_{1v}	$2\Sigma_1$	C_{1v}	$4\Sigma_1$
u	C_1	$2u$	C_1	$4u$

TABLE V. Selection rules for electron-radiation interaction with $\hat{x}$ and $\hat{y}$ light polarization in monolayer and N-layer graphenes [see Fig. 1(g) for $\hat{x}$ and $\hat{y}$ definition].

	BZ point	Polarization	$W(k)$
Monolayer	T	$x \in T_3$	$T_2\otimes T_3\otimes T_4$ non null
		$y \in T_1$	$T_2\otimes T_1\otimes T_4$ null
	u	$x, y \in u^+$	$u^-\otimes u^+\otimes u^-$ non null
Gated monolayer	T	$x \in T_2$	$T_1\otimes T_2\otimes T_2$ non null
		$y \in T_1$	$T_1\otimes T_1\otimes T_2$ null
	u	$x, y \in u$	$u\otimes u\otimes u$ non null
N even	T	$x \in T_2$	$T_1\otimes T_2\otimes T_1$ null
			$T_1\otimes T_2\otimes T_2$ non null
			$T_2\otimes T_2\otimes T_2$ null
		$y \in T_1$	$T_1\otimes T_1\otimes T_1$ non null
			$T_1\otimes T_1\otimes T_2$ null
			$T_2\otimes T_1\otimes T_2$ non null
	u	$x, y \in u$	$u\otimes u\otimes u$ non null
Biased bilayer	T	$x, y \in T$	$T\otimes T\otimes T$ non null
	u	$x, y \in u$	$u\otimes u\otimes u$ non null
N odd	T	$x, y \in T^+$	$T^+\otimes T^+\otimes T^+$ non null
			$T^+\otimes T^+\otimes T^-$ null
			$T^-\otimes T^+\otimes T^-$ non null
	u	$x, y \in u^+$	$u^+\otimes u^+\otimes u^+$ non null
			$u^+\otimes u^+\otimes u^-$ null
			$u^-\otimes u^+\otimes u^-$ non null

The bilayer graphene is composed by four electronic bands at the T line, belonging to two T_1 and two T_2 irreducible representations. The four possible transitions are illustrated in Figs. 3(a) and 3(b). In this case both x and y polarized lights can be absorbed. For the biased bilayer graphene, all electronic representations are the same, and it contains both x,y base functions for light polarizations. Thus, all four transitions are allowed to connect all four bands by the same light polarization, differently from the unbiased bilayer case

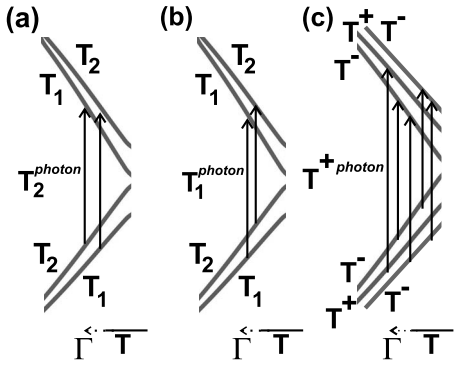

FIG. 3. [(a) and (b)] Schematic electron dispersion of bilayer graphene along the $K\Gamma$ direction showing the possible transition induced by (a) a photon with T_2 symmetry (x polarization) and (b) a T_1 photon (y polarization). (c) The electronic dispersion of trilayer graphene showing the five possible transitions induced by light absorption.

TABLE VI. Allowed processes for electron-phonon scattering for monolayer and N-layer graphenes, along the T and T' lines and at a generic u point, for each phonon symmetry.

	BZ point	Phonon	Allowed scattering
Monolayer	$T(T')$	T_1	$T_2 \to T_2$, $T_4 \to T_4$
		T_3	$T_2 \to T_4$
	u	u^+	$u^- \to u^-$
Gated monolayer	$T(T')$	T_1	$T_1 \to T_1$, $T_2 \to T_2$
		T_2	$T_1 \to T_2$
	u	u	$u \to u$
N even	$T(T')$	T_1	$T_1 \to T_1$, $T_2 \to T_2$
		T_2	$T_1 \to T_2$
	u	u	$u \to u$
Biased bilayer	$T(T')$	T	$T \to T$
	u	u	$u \to u$
N odd	$T(T')$	T^+	$T^+ \to T^+$, $T^- \to T^-$
		T^-	$T^+ \to T^-$
	u	u^+	$u^+ \to u^+$, $u^- \to u^-$
		u^-	$u^+ \to u^-$

where the light polarization selects the pair of bands that can be connected.

The trilayer graphene will have more possibilities for light induced transitions since there are more possibilities between the three π and three π^* bands. Along $T(T')$ direction, there are two T^+ and four T^- bands giving rise to five possible transitions, as shown in Fig. 3(c).

IV. SELECTION RULES FOR THE FIRST-ORDER RAMAN SCATTERING AND INFRARED ABSORPTION PROCESSES

The first-order Raman-scattering process is limited to phonons at the center of BZ (Γ point) due to momentum conservation requirement (phonon wave vector $q=0$). In monolayer graphene the first-order Raman spectra is composed by the G band vibrational mode, which is doubly degenerated at the Γ point with Γ_6^+ symmetry. The Raman-active modes depending on N ($N>1$) (without acoustic modes) are

$$\Gamma^{\text{Raman}} = N(\Gamma_3^+ + \Gamma_1^+), \quad \text{for } N \text{ even},$$

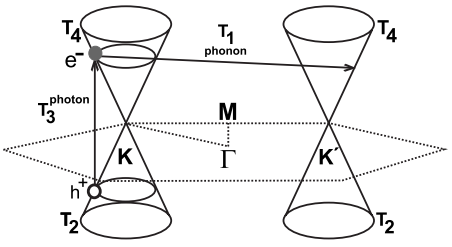

FIG. 4. The most efficient DRR process in graphene showing the absorption of light with polarization symmetry T_3, followed by electron scattering by a phonon with T_1 symmetry.

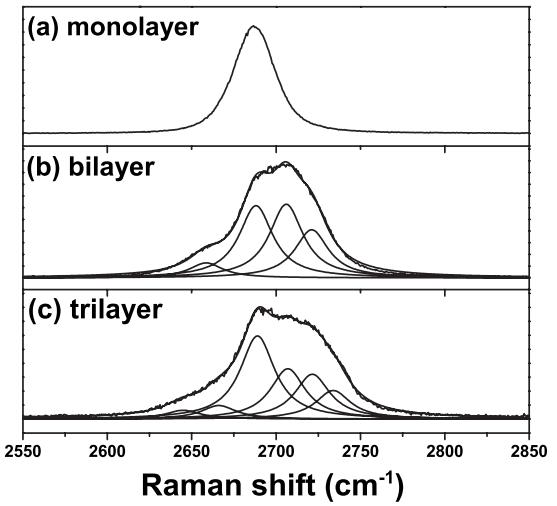

FIG. 5. The measured Raman spectra of the G' band of a (a) monolayer, (b) bilayer, and (c) trilayer graphenes. The samples were made by exfoliating graphite on top of a 100 nm silicon oxide substrate using 2.41 eV laser energy. The G' band for monolayer, bilayer, and trilayer graphenes were fitted with one, four, and six Lorentzians, respectively, with a FWHM of 24 cm^{-1}.

$$\Gamma^{\text{Raman}} = N\Gamma_3^+ + (N-1)(\Gamma_3^- + \Gamma_1^+), \quad \text{for } N \text{ odd}.$$

For even number of layers, the G band belongs to the Γ_3^+. There is a low-frequency Γ_3^+ mode with frequency depending on the number of layers (35–53 cm^{-1}).[34] Two new Raman-active modes near ~80 and ~900 cm^{-1} appear with Γ_1^+ irreducible representations.[34,35] For odd number of layers the G band is assigned as a combination of Γ_3^+ and Γ_3^- representations; also the smaller wave-number component is active in Raman by a Γ_1^+ representation.

For monolayer graphene there is an IR active mode belonging to the Γ_2^- representation, giving rise to an absorption near ~870 cm^{-1}. The IR active modes for $N>1$ are

$$\Gamma^{\text{IR}} = (N-1)\Gamma_2^- + (N-1)\Gamma_3^-, \quad \text{for } N \text{ even},$$

$$\Gamma^{\text{IR}} = N(\Gamma_3^+ + \Gamma_2^-), \quad \text{for } N \text{ odd}.$$

For even number of layers the active modes belong to the Γ_2^- and Γ_3^- representations, with the latter one referring to the ~1590 cm^{-1} frequency vibration.[34,35] The infrared-active

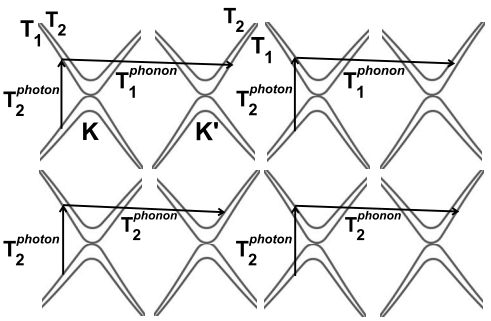

FIG. 6. The four allowed DRR processes in bilayer graphene, taking into account the optical anisotropy.

TABLE VII. Example of irreducible representation notation conversion from the Γ-point space group to D_{3h} and D_{3d} point groups, and from the K–point space group to C_{3h} and D_3 point groups.

Γ point				K point			
D_{3h}		D_{3d}		C_{3h}		D_3	
SG	PG	SG	PG	SG	PG	SG	PG
Γ_1^+	A_1'	Γ_1^+	A_{1g}	K_1^+	A'	K_1	A_1
Γ_1^-	A_1''	Γ_1^-	A_{1u}	K_1^-	A''	K_2	A_2
Γ_2^+	A_2'	Γ_2^+	A_{2g}	K_2^+	E'	K_3	E
Γ_2^-	A_2''	Γ_2^-	A_{2u}	K_2^{+*}	E'^*		
Γ_3^+	E'	Γ_3^+	E_g	K_2^-	E''		
Γ_3^-	E''	Γ_3^-	E_u	K_2^{-*}	E''^*		

modes for odd layer number belong to Γ_2^- and Γ_3^+ which are also Raman active.

V. ELECTRON SCATTERING BY $q \neq 0$ PHONONS AND THE DOUBLE RESONANCE RAMAN SCATTERING

The EPS is calculated from the initial and final electron wave functions coupled by the phonon eigenvector[36,37] using the phonon-induced deformation potential. Therefore, the selection rules of the EPS processes are obtained by the direct product of the symmetries of the initial and final electronic states, and the symmetry of the phonon involved in the process. The allowed electron-phonon scattering processes for monolayer, gated monolayer, N-even, biased bilayer, and N-odd, along the $K\Gamma$ and KM directions (T and T' lines, respectively) and at a generic u point, are summarized in Table VI.

One example of explicit use of the electron-radiation and EPS selection rules is the double-resonance Raman-scattering process,[38,39] in which an electron in the conduction band is scattered by a phonon with wave vector outside the Γ point in an intervalley (connecting electronic states near the K and K' points) or in an intravalley (connecting electronic state near the same K or K' point) process. The G' Raman band ($\sim$2700 cm^{-1}) comes from an intervalley process in which the electron is scattered by an in-plane transversal optic (iTO) phonon.[40] We will discuss in detail the G' scattering for monolayer, bilayer, and trilayer graphenes.

For the monolayer graphene, a possible scattering is illustrated in Fig. 4. The iTO phonon at the KM (T') direction presents a T_1 symmetry, which can only connect two electrons with the same symmetry. Many other similar scattering events are allowed by symmetry, involving electrons/holes in the $K\Gamma$ (T) direction or at any general u point inside the circle defined by the T_3 photon energy. However, the matrix element has a strong angular dependence and the scattering is dominated by the T electrons, as discussed in Ref. 9. Therefore, the G' Raman band has only one peak, with full width at half maximum (FWHM) of $\sim$24 cm^{-1} [see Fig. 5(a)].[4,9] For the graphene on top of a substrate, the same selection rules apply, and the expected number of G' peaks is the same as for the isolated monolayer graphene on an isotropic medium.

For the bilayer graphene, the number of allowed DRR processes predicted by group theory will be larger since both electronic and phonon branches are doubled. Along the T line, there is polarization dependence for the absorption linking different electronic bands, as discussed in Sec. III. For wave vectors in the range of visible-light energy, the electron dispersion are almost linear, then optical anisotropy can be applied here as for monolayer graphene.[41] Now, for computing the number of resonant conditions involved in the DRR process, we are left with only two excited electronic bands with symmetries T_1 and T_2, which corresponds to Fig. 3(a). The iTO phonons for bilayer graphene have T_1 and T_2 symmetries. For the electron scattering by a T_1 phonon, the allowed process is between K and K' electronic bands with same symmetry ($T_1 \rightarrow T_1$ or $T_2 \rightarrow T_2$). The same happens with the electron scattering by a T_2 phonon but it connects conduction bands of different symmetries, i.e., $T_1 \rightleftarrows T_2$. This gives rise to four possible DRR processes, as shown in Fig. 6.[4] The Raman spectra can then be used to differentiate monolayer and bilayer graphenes (see Fig. 5).[4–6]

In the case of biased bilayer graphene, there are no selection rules involving different photon polarizations. The biased bilayer can have photon absorption linking all valence and conduction bands. This leads to eight possible transitions considering EPS selection rules for T_1 and T_2 phonons.

For the trilayer graphene, the DRR process will have again more contributions because each phonon and electron band will be split in three levels. Along the T line, there are five possibilities linking the electronic bands between the K and K' points with a T^+ phonon, and four possibilities for the T^- phonon. The total number of DRR process predicted by group theory will be fifteen. However, the FWHM is large when compared to the energy splitting between the G' Raman peaks, and when one makes measurements of the G' Raman band in trilayer graphene, these fifteen peaks cannot be distinguished, as illustrated in Fig. 5(c). Similar problem should happen for $N \geq 4$.

VI. SUMMARY

In this work we analyzed the symmetry aspects related to electrons and phonons at each point in the BZ of graphene, depending on the number of layers. The symmetry aspects can be generalized to any value of N, differing for N even or odd. For monolayer and bilayer, we consider both an isotropic and an anisotropic medium. We derived the selection rules for electron-radiation and electron-phonon interactions. Some specific findings can be remarked: (i) for the monolayer graphene, the predicted optical anisotropy[31] comes out directly from group theory analysis. The electron-phonon scattering process is allowed by symmetry at any generic point (u) in the Dirac cone, and the observation of a single Lorentzian in the G' Raman band comes from a strong anisotropy in the electron-phonon matrix element.[9] (ii) The gated graphene has lower symmetry but the optical anisotropy is still present. Moreover for the DRR process, the symmetry considerations are the same as graphene on an

isotropic medium. (iii) In the case of bilayer graphene, the optical anisotropy is also present and there are four dominant processes in the DRR. This number increases to eight on biased bilayer. (iv) In trilayer graphene, the number of possible DRR processes is 15. However, the 15 processes are not distinguishable and the G' Raman band can be nicely fit with six Lorentzians. A similar situation is expected for a larger number of layers.

ACKNOWLEDGMENTS

We would like to thank M. A. Pimenta, J. F. Sampaio, L. G. Cançado, E. B. Barros, and R. W. Nunes for useful discussions. This work was supported by Rede Nacional de Pesquisa em Nanotubos de Carbono-MCT, FAPEMIG, and CNPq.

APPENDIX: NOTATION CONVERSION FROM SPACE-GROUP TO POINT-GROUP IRREDUCIBLE REPRESENTATIONS

In this work we derived the Γ_π and $\Gamma_{\text{lat vib}}$ for all points in the first BZ of multilayer graphene, maintaining the notation of SG for the irreducible representations. The conversion to PG representation is obtained considering that (a) superscript sign "+" or "−" applies if the character of the horizontal mirror (σ_h) or inversion (i) is positive or negative, respectively; (b) the subscript number is given following the order of the point-group irreducible representations according to Tables in Ref. 3; (c) two representations can only have the same number if they have superscript with positive or negative signs. As an example we give in Table VII the Γ point space-group notation conversion to the D_{3h} (N-odd) and D_{3d} (N-even) point groups, and for the K point space group to the C_{3h} (N-odd) and D_3 (N-even) point groups.

[1] A. K. Geim and K. S. Novoselov, Nature Mater. **6**, 183 (2007).
[2] A. H. Castro Neto, F. Guinea, N. M. R. Peres, K. S. Novoselov, and A. K. Geim, Rev. Mod. Phys. **81**, 109 (2009).
[3] M. S. Dresselhaus, G. Dresselhaus, and A. Jorio, *Group Theory: Application to the Physics of Condensed Matter* (Springer-Verlag, Heidelberg, 2008).
[4] A. C. Ferrari, J. C. Meyer, V. Scardaci, C. Casiraghi, M. Lazzeri, F. Mauri, S. Piscanec, D. Jiang, K. S. Novoselov, S. Roth, and A. K. Geim, Phys. Rev. Lett. **97**, 187401 (2006).
[5] A. Gupta, G. Chen, P. Joshi, S. Tadigadapa, and P. C. Eklund, Nano Lett. **6**, 2667 (2006).
[6] D. Graf, F. Molitor, K. Ensslin, C. Stampfer, A. Jungen, C. Hierold, and L. Wirtz, Nano Lett. **7**, 238 (2007).
[7] L. M. Malard, J. Nilsson, D. C. Elias, J. C. Brant, F. Plentz, E. S. Alves, A. H. Castro Neto, and M. A. Pimenta, Phys. Rev. B **76**, 201401(R) (2007).
[8] Z. Ni, Y. Wang, T. Yu, Y. You, and Z. Shen, Phys. Rev. B **77**, 235403 (2008).
[9] D. L. Mafra, G. Samsonidze, L. M. Malard, D. C. Elias, J. C. Brant, F. Plentz, E. S. Alves, and M. A. Pimenta, Phys. Rev. B **76**, 233407 (2007).
[10] E. McCann and V. I. Fal'ko, Phys. Rev. Lett. **96**, 086805 (2006).
[11] T. Ohta, A. Bostwick, T. Seyller, K. Horn, and E. Rotenberg, Science **313**, 951 (2006).
[12] E. V. Castro, K. S. Novoselov, S. V. Morozov, N. M. R. Peres, J. M. B. Lopes dos Santos, J. Nilsson, F. Guinea, A. K. Geim, and A. H. Castro Neto, Phys. Rev. Lett. **99**, 216802 (2007).
[13] E. McCann, Phys. Rev. B **74**, 161403(R) (2006).
[14] J. Nilsson, A. H. Castro Neto, F. Guinea, and N. M. R. Peres, Phys. Rev. B **76**, 165416 (2007).
[15] R. Saito, G. Dresselhaus, and M. S. Dresselhaus, *Physical Properties of Carbon Nanotubes* (Imperial College Press, London, 1998).
[16] K. Kechedzhi, E. McCann, V. I. Fal'ko, H. Suzuura, T. Ando, and B. L. Altshuler, Eur. Phys. J. Spec. Top. **148**, 39 (2007).
[17] W. Kohn and L. J. Sham, Phys. Rev. **140**, A1133 (1965).
[18] P. Ordejón, E. Artacho, and J. M. Soler, Phys. Rev. B **53**, R10441 (1996).
[19] J. M. Soler, E. Artacho, J. D. Gale, A. Garcia, J. Junquera, P. Ordejón, and D. Sánchez-Portal, J. Phys.: Condens. Matter **14**, 2745 (2002).
[20] J. W. McClure, Phys. Rev. **108**, 612 (1957).
[21] J. C. Slonczewski and P. R. Weiss, Phys. Rev. **109**, 272 (1958).
[22] T. Ohta, A. Bostwick, J. L. McChesney, T. Seyller, K. Horn, and E. Rotenberg, Phys. Rev. Lett. **98**, 206802 (2007).
[23] M. Koshino and E. McCann, arXiv:0809.0983 (unpublished).
[24] B. Partoens and F. M. Peeters, Phys. Rev. B **74**, 075404 (2006).
[25] S. Latil and L. Henrard, Phys. Rev. Lett. **97**, 036803 (2006).
[26] J. L. Mañes, F. Guinea, and M. A. H. Vozmediano, Phys. Rev. B **75**, 155424 (2007).
[27] K. S. Novoselov, A. K. Geim, S. V. Morozov, D. Jiang, Y. Zhang, S. V. Dubonos, I. V. Grigorieva, and A. A. Firsov, Science **306**, 666 (2004).
[28] Y. Zhang, Y. Tan, H. L. Stormer, and P. Kim, Nature (London) **438**, 201 (2005).
[29] C. Casiraghi, S. Pisana, K. S. Novoselov, A. K. Geim, and A. C. Ferrari, Appl. Phys. Lett. **91**, 233108 (2007).
[30] P. Y. Yu and M. Cardona, *Fundamentals of Semiconductors: Physics and Materials Properties* (Springer-Verlag, Heidelberg, 2005).
[31] A. Grüneis, R. Saito, Ge. G. Samsonidze, T. Kimura, M. A. Pimenta, A. Jorio, A. G. Souza Filho, G. Dresselhaus, and M. S. Dresselhaus, Phys. Rev. B **67**, 165402 (2003).
[32] L. G. Cançado, M. A. Pimenta, B. R. A. Neves, G. Medeiros-Ribeiro, T. Enoki, Y. Kobayashi, K. Takai, K. I. Fukui, M. S. Dresselhaus, R. Saito, and A. Jorio, Phys. Rev. Lett. **93**, 047403 (2004).
[33] L. G. Cançado, M. A. Pimenta, B. R. A. Neves, M. S. S. Dantas, and A. Jorio, Phys. Rev. Lett. **93**, 247401 (2004).
[34] S. K. Saha, U. V. Waghmare, H. R. Krishnamurthy, and A. K. Sood, Phys. Rev. B **78**, 165421 (2008).
[35] J. W. Jiang, H. Tang, B. S. Wang, and Z. B. Su, Phys. Rev. B **77**, 235421 (2008).
[36] J. Jiang, R. Saito, A. Grüneis, S. G. Chou, Ge. G. Samsonidze,

A. Jorio, G. Dresselhaus, and M. S. Dresselhaus, Phys. Rev. B **71**, 205420 (2005).
[37] A. H. Castro Neto and F. Guinea, Phys. Rev. B **75**, 045404 (2007).
[38] C. Thomsen and S. Reich, Phys. Rev. Lett. **85**, 5214 (2000).
[39] R. Saito, A. Jorio, A. G. Souza Filho, G. Dresselhaus, M. S. Dresselhaus, and M. A. Pimenta, Phys. Rev. Lett. **88**, 027401 (2001).
[40] J. Maultzsch, S. Reich, C. Thomsen, H. Requardt, and P. Ordejón, Phys. Rev. Lett. **92**, 075501 (2004).
[41] L. G. Cançado, A. Reina, J. Kong, and M. S. Dresselhaus, Phys. Rev. B **77**, 245408 (2008).